Cell Reports

Report

Apparent RNA bridging between PRC2 and chromatin is an artifact of non-specific chromatin precipitation upon RNA degradation

Graphical abstract

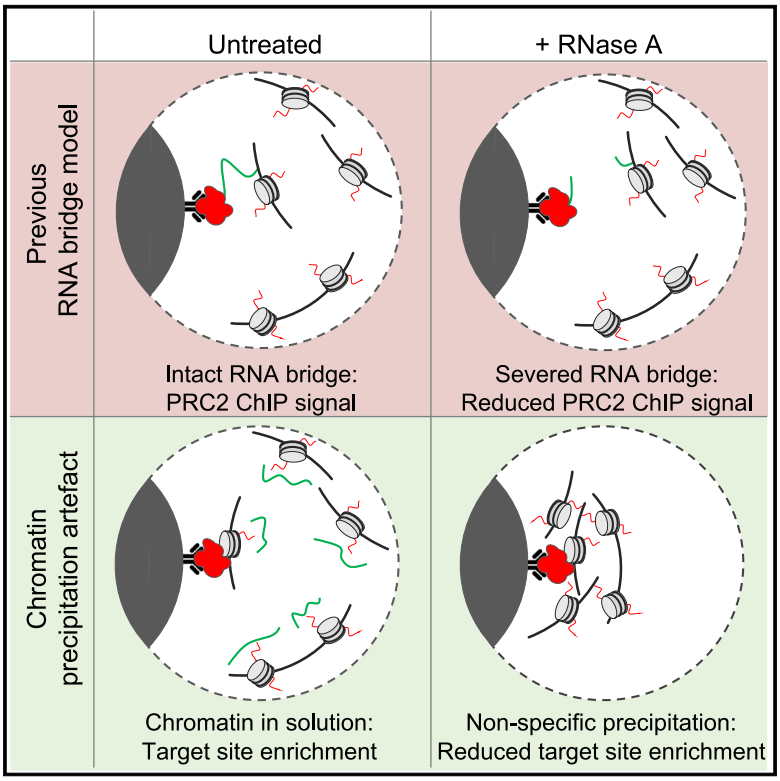

Authors

Alexander Hall Hickman, Richard G. Jenner

Correspondence

r.jenner@ucl.ac.uk

In brief

The reduced detection of PRC2 target sites upon the addition of RNase A to chromatin immunoprecipitation experiments suggests the existence of RNA bridges that connect PRC2 to chromatin. Hall Hickman and Jenner report that this effect is an artifact of non-specific chromatin precipitation that occurs upon RNA degradation.

Highlights

- rChIP has suggested the presence of RNA bridges that connect PRC2 to chromatin
- RNase A treatment in rChIP experiments causes non-specific chromatin precipitation
- Non-specific precipitation masks enrichment of sites of PRC2 and H3K27me3 occupancy
- PGA prevents background precipitation and rescues detection of chromatin occupancy

Hall Hickman & Jenner, 2024, Cell Reports *43*, 113856
March 26, 2024
https://doi.org/10.1016/j.celrep.2024.113856

CellPress

Cell Reports

CellPress
OPEN ACCESS

Report

Apparent RNA bridging between PRC2 and chromatin is an artifact of non-specific chromatin precipitation upon RNA degradation

Alexander Hall Hickman[1,2] and Richard G. Jenner[1,2,3,*]
[1]UCL Cancer Institute, University College London, London WC1E 6BT, UK
[2]CRUK City of London Centre, University College London, London WC1E 6BT, UK
[3]Lead contact
*Correspondence: r.jenner@ucl.ac.uk
https://doi.org/10.1016/j.celrep.2024.113856

SUMMARY

Polycomb repressive complex 2 (PRC2) modifies chromatin to maintain repression of genes specific for other cell lineages. *In vitro*, RNA inhibits PRC2 activity, but the effect of RNA on PRC2 in cells is less clear, with studies concluding that RNA either antagonizes or promotes PRC2 chromatin association. The addition of RNase A to chromatin immunoprecipitation reactions has been reported to reduce detection of PRC2 target sites, suggesting the existence of RNA bridges connecting PRC2 to chromatin. Here, we show that the apparent loss of PRC2 chromatin association after RNase A treatment is due to non-specific chromatin precipitation. RNA degradation precipitates chromatin out of solution, thereby masking enrichment of specific DNA sequences in chromatin immunoprecipitation reactions. Maintaining chromatin solubility by the addition of poly-L-glutamic acid rescues detection of PRC2 chromatin occupancy upon RNA degradation. These findings undermine support for the model that RNA bridges PRC2 and chromatin in cells.

INTRODUCTION

Chromatin regulation is fundamental for cell identity and cell differentiation. Chromatin modifiers open chromatin at genes important for the cell's identity and close chromatin at genes specific for other cell types, and this is regulated dynamically during cell differentiation. Dysregulation of these processes causes developmental disorders and cancer.[1,2] Chromatin is associated with a host of RNA species, including nascent RNAs in the process of transcription and a subset of mature transcripts that remain localized to the nucleus.[3–5] It has become apparent that RNA interacts with chromatin modifiers and modulates their association with chromatin, but the mechanisms underlying these effects remain poorly understood.[4–9]

Polycomb repressive complex 2 (PRC2) has become a paradigm for RNA binding chromatin regulators.[6–9] PRC2 associates with genes specific for other cell lineages and maintains them in a silent state.[10,11] PRC2 is recruited to chromatin through the interaction of accessory subunits with ubiquitinated histone H2A (H2AK119ub) and with GC-rich sequences located at CpG islands.[10,11] The PRC2 enzymatic subunit EZH2 trimethylates histone H3 at lysine 27 (H3K27me3), which creates a binding site for canonical forms of PRC1 and allosterically activates PRC2 activity through its subunit EED.

That PRC2 also binds RNA was first reported for certain long non-coding RNA species, which were proposed to recruit PRC2 to specific sites on chromatin.[12–15] Subsequently, PRC2 was found to interact primarily with nascent pre-mRNAs in cells with a preference for G-tract sequences, especially when folded into G-quadruplex structures.[16–22] *In vitro*, RNA inhibits PRC2 catalytic activity[22–24] by antagonizing its interaction with DNA,[25] nucleosomes,[17] and the substrate H3 tail[19] and by blocking allosteric activation through EED.[26]

The effect of RNA on PRC2 function in cells has been less clear. Consistent with *in vitro* data, tethering G-tract RNA to polycomb target genes reduces PRC2 occupancy and depletes H3K27me3 in *cis*.[19] Other studies have concluded that RNA can also promote PRC2's repressive effects on chromatin in cells.[20,27] One of the seemingly strongest pieces of evidence that RNA plays a positive role in PRC2 chromatin association in cells is from experiments by Long and colleagues utilizing a variant of chromatin immunoprecipitation coupled with sequencing (ChIP-seq) methodology, termed rChIP.[27] The authors found that the addition of RNase A during the IP step abrogated detection of PRC2 chromatin occupancy but had no effect on RNA polymerase II or TBP. These data were interpreted as RNase A severing an RNA "bridge" that tethered PRC2 to its target sites on chromatin.

To understand further the mechanism by which RNA regulates PRC2 chromatin occupancy, we probed the effect of RNase A treatment on chromatin in ChIP reactions. We found that the apparent loss of PRC2 chromatin occupancy that occurs upon RNase A treatment stems from non-specific precipitation of chromatin rather than the loss of PRC2-bound genomic fragments. Our results thus undermine support for the model that RNA bridges PRC2 and chromatin in cells and have implications for other studies that employ RNase A in a similar manner.

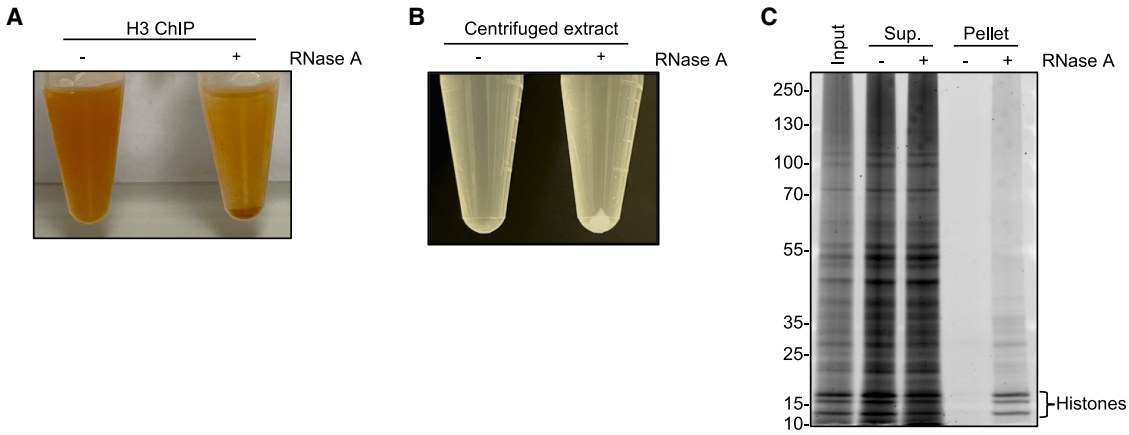

Figure 1. The RNase A treatment step in rChIP methodology precipitates chromatin from solution

(A) Aggregation and sedimentation of protein A/G magnetic beads during rChIP for histone H3 in RNase A-treated sonicated crosslinked mouse embryonic stem cell (mESC) extract. Representative of 2 independent experiments.

(B) Presence of an insoluble pellet after centrifugation of sonicated mESC extract prepared according to rChIP methodology following incubation with RNase A. Representative of 2 independent experiments.

(C) SDS-PAGE of equal volumes of input, supernatant (sup.), and pelleted fractions isolated from centrifuged sonicated crosslinked mESC extract treated or not treated with RNase A. Histones are marked. Representative of 2 independent experiments.

RESULTS

The RNase A treatment step in rChIP methodology precipitates chromatin from solution

In seeking to understand the basis of the results of the rChIP method, we performed rChIP for histone H3 in mouse embryonic stem cells. Sonicated crosslinked cell extracts were prepared as described,[27] and anti-histone H3 antibody added, before the sample was split in two; RNase A was added to one of the tubes, and both samples were incubated overnight. After the subsequent addition of protein A/G beads to the tubes, we noticed a clear aggregation of the beads in the sample treated with RNase A (Figure 1A). Investigating this phenomenon further in the absence of antibody and beads, we found that RNase A treatment caused precipitation of material from the extracts that could be visualized as a large pellet after centrifugation (Figure 1B). SDS-PAGE demonstrated that this insoluble, pelleted material was enriched in histones, which were correspondingly depleted from the supernatant by RNase A treatment (Figure 1C). These results indicate that RNase A treatment of sonicated cell extracts in the rChIP procedure causes the precipitation of chromatin from solution.

Poly-L-glutamic acid (PGA) maintains chromatin solubility upon RNA degradation

RNA degradation caused by RNase A treatment has previously been reported to cause precipitation of histones from sonicated cell extracts because the loss of polyanionic RNA allows the formation of electrostatic interactions between positively charged histone tails and DNA.[28,29] It was also found that histone solubility could be restored in these conditions by the addition of the alternative anionic polymer PGA.[28] We therefore tested whether the addition of PGA would prevent chromatin from precipitating during the rChIP procedure. We found that the addition of PGA immediately prior to RNase A prevented precipitation of proteins, including histones, upon RNase A treatment (Figure 2A). We also found that RNase A treatment precipitated DNA from solution and that this too was prevented by PGA addition (Figure 2B). PGA had no effect on the ability of RNase A to degrade RNA in nuclear extracts (Figure 2C), demonstrating that PGA did not maintain chromatin solubility by inhibiting RNase A activity.

To characterize the nature of the RNase A-induced insoluble material further, we subjected the pellet and supernatant to immunoblotting (Figure 2D). This confirmed that the insoluble material was enriched for histone H3, including H3 trimethylated at lysine 27 (H3K27me3), and contained the PRC2 subunit EZH2. The RNA polymerase II subunit RPB1 was also present in the pellet but was not as enriched as EZH2 or H3. Furthermore, PGA reduced the precipitation of histone H3, EZH2, and RPB1 caused by RNase A treatment. These results demonstrate that the RNA degradation step in the rChIP protocol causes chromatin and its associated proteins to precipitate from solution and that the addition of an alternative anionic polymer in the form of PGA prevents this from occurring.

RNase A treatment reduces the specificity of IP reactions

We next tested whether chromatin precipitation in the presence of RNase A affected IP specificity. We performed co-immunoprecipitation (coIP) for histone H3, the PRC2 subunit SUZ12, and RPB1 in the presence and absence of RNase A and blotted for these factors in the input and IP fractions (Figure 3A). In the absence of RNase A, each IP reaction specifically enriched its target protein, as expected. However, in the presence of RNase A, the IP reactions exhibited reduced specificity, pulling down other factors. In the presence of RNase A, IP for H3 enriched for EZH2, H3K27me3, and H3K27ac, while IPs for SUZ12 and RPB1 also enriched for H3, H3K27me3, and H3K27ac (Figure 3A). The addition of PGA with RNase A increased the

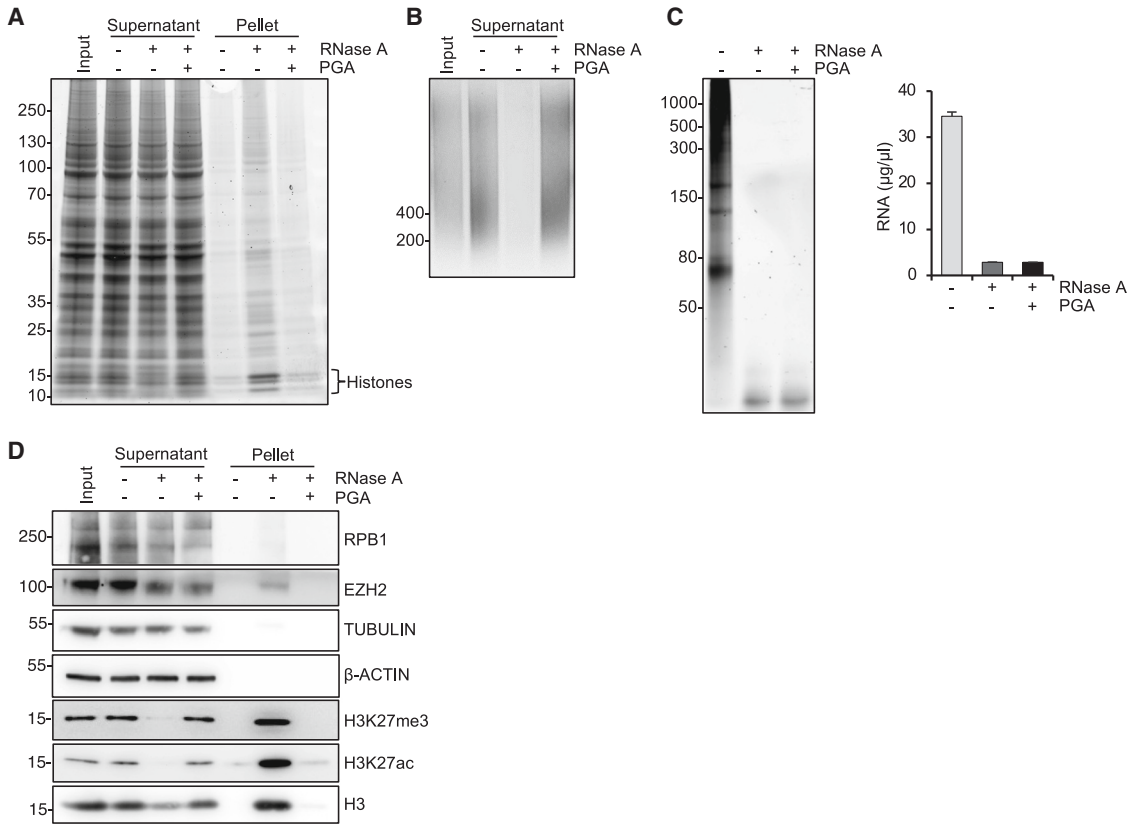

Figure 2. PGA maintains chromatin solubility upon RNA degradation

(A) SDS-PAGE of equal volumes of input, sup., and pelleted fractions isolated from centrifuged sonicated mESC extract treated with RNase A alone or RNase A and PGA (400 ng/μL) or left untreated. Representative of 2 independent experiments.

(B) Agarose gel electrophoresis of equal volumes of DNA purified from the sups. of the samples described in (A). Representative of 2 independent experiments.

(C) Left: TBE-urea PAGE of RNA purified from sonicated mESC extract treated with RNase A alone or RNase A and PGA or left untreated. The dashes mark the position of single-stranded RNA (ssRNA) size markers. Right: concentration of purified RNA (mean and SEM, 3 independent experiments).

(D)Immunoblots for the indicated proteins in the samples described in (A). Representative of 2 independent experiments.

specificity of each IP. Thus, these data show that the precipitation of chromatin out of solution caused by RNase A in the rChIP procedure reduces the specificity of IP reactions by increasing the amount of background material that is co-precipitated.

We hypothesized that the increase in non-specific chromatin precipitation upon RNase A treatment would reduce the specificity of DNA enrichment by ChIP. To test this, we performed rChIP for SUZ12, H3K27me3, and RPB1 and measured enrichment of the repressed PRC2 target genes *Hoxd11* and *Bmp6* and the active housekeeping genes *Actb* and *Gapdh* by qPCR (Figure 3B). In the absence of RNase A, we found that ChIP for SUZ12 and H3K27me3 enriched for *Hoxd11* and *Bmp6*, but not for *Actb* or *Gapdh*, as expected. Reciprocally, ChIP for RPB1 enriched for *Actb* and *Gapdh* but not for *Hoxd11* and *Bmp6*. Then, examining the enrichment of these genes in samples treated with RNase A, we found increased precipitation of *Hoxd11* and *Bmp6* in H3K27me3 ChIPs with a smaller effect for SUZ12. However, this was coupled with a larger increase in precipitation of *Gapdh* and *Actb* in both SUZ12 and H3K27me3 ChIPs ($p < 0.05$, t test). Reciprocally, RNase A treatment increased precipitation of *Hoxd11* and *Bmp6* by RPB1 ChIP, although this did not reach significance. Calculating the ratio of *Hoxd11* and *Bmp6* versus *Gapdh* as a measure of ChIP specificity demonstrated that RNase A treatment significantly reduced the specificity of SUZ12, H3K27me3, and RPB1 ChIPs: RNase A treatment reduced the fold enrichment of *Hoxd11* and *Bmp6* versus *Gapdh* in SUZ12 and H3K27me3 ChIPs from between ~20- and 60-fold to ~3- to 5-fold ($p < 0.05$; Figure 3C). Reciprocally, RNase A treatment increased enrichment of *Hoxd11* and *Bmp6* versus *Gapdh* in RPB1 ChIPs. In the presence of PGA, the specificity of each ChIP was re-established to levels similar to that observed in the absence of RNase A (RNase A + PGA versus RNase A, $p < 0.05$; RNase A + PGA versus untreated, $p > 0.05$; Figure 3C). We conclude, consistent with our coIP data, that RNase A treatment in the rChIP protocol reduces the specify of IP reactions by increasing the background, non-specific precipitation of chromatin.

Apparent RNA-dependent PRC2 occupancy in rChIP experiments is due to non-specific chromatin IP

In rChIP and other ChIP-seq experiments, the number of sequencing reads at each genomic position is relative to the total

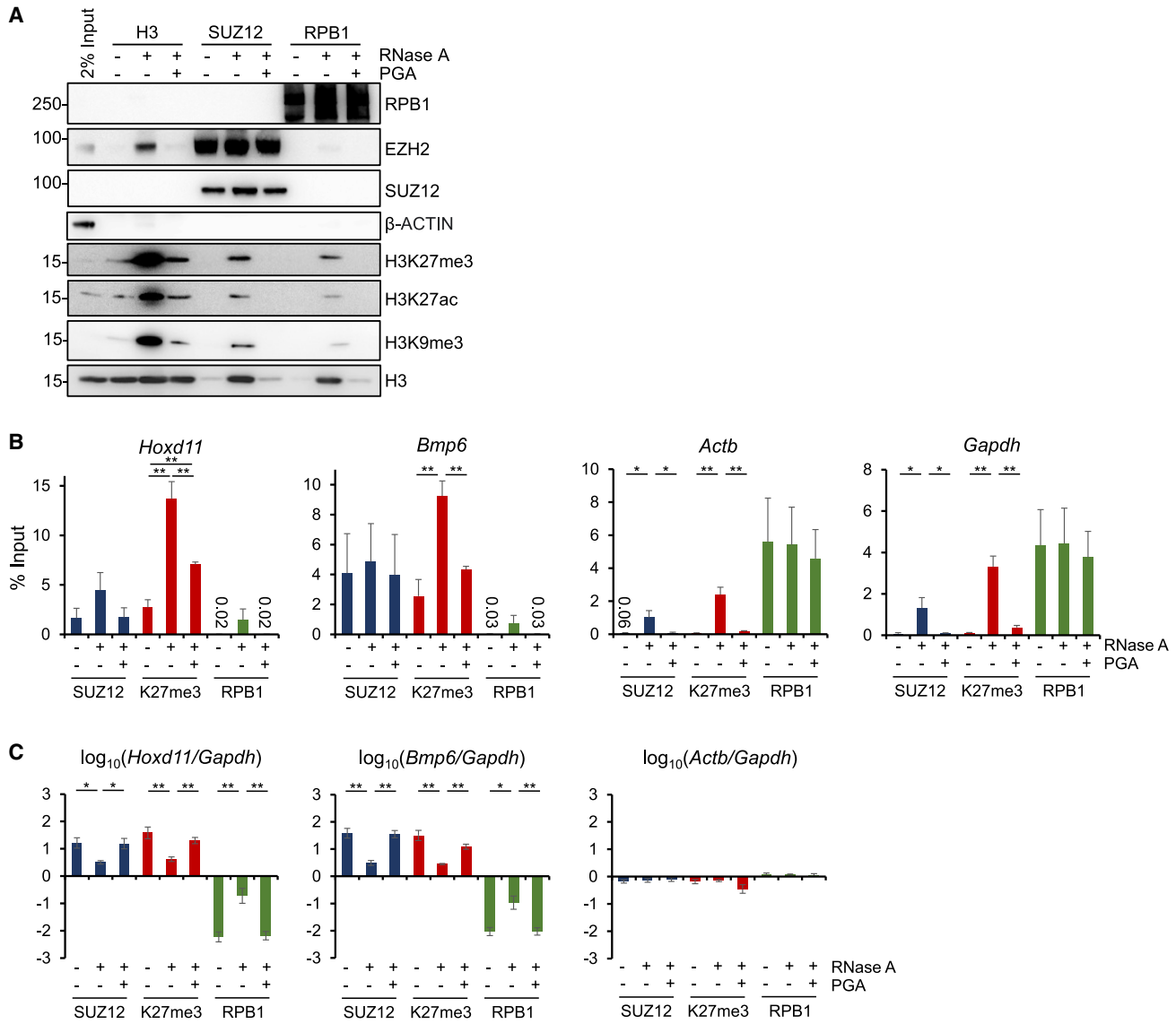

Figure 3. RNase A treatment reduces the specificity of IP reactions

(A) Immunoblots of the indicated proteins in input and H3, SUZ12, and RPB1 IPs from sonicated crosslinked mESC extracts after treatment with RNase A or RNase A and PGA or left untreated. Representative of 2 independent experiments.

(B) Quantitative PCR (as percentage of input) for *Hoxd11*, *Bmp6*, *Actb*, and *Gapdh* in SUZ12, H3K27me3, and RPB1 rChIP samples from mock-, RNase A-, or RNase A and PGA-treated sonicated crosslinked mESC extracts (mean and SEM, 3 independent experiments; pairwise comparisons between conditions for each factor: *$p < 0.05$ and **$p < 0.01$; one-sided t test).

(C) Data in (B) except normalized to *Gapdh*.

number of reads and, because of this, observation of genome occupancy requires enrichment relative to the genomic background. Thus, we considered that the increase in pull down of non-specific genomic DNA upon RNase A treatment could render ChIP samples essentially equivalent to whole-genome input samples, accounting for the apparent loss of PRC2 occupancy at its target genes observed by Long et al.[27] We hypothesized that if this was the case, then RNase A treatment should have the same apparent effect on H3K27me3 occupancy, even though this histone modification is not considered to be attached to chromatin via an RNA bridge. We also hypothesized that the apparent effects of RNase A on PRC2 and H3K27me3 chromatin occupancy should largely be prevented by the addition of PGA.

To test these theories, we performed rChIP for SUZ12 and H3K27me3, and also for RPB1, used by Long et al. as a presumed RNA-independent control. We found that RNase A treatment resulted in the loss of enrichment of PRC2-occupied sites (Figures 4A, 4B, and S1), mimicking the apparent RNA-dependent SUZ12 and EZH2 occupancy reported by Long et al. We also found that RNase A treatment had an identical

CellPress
OPEN ACCESS

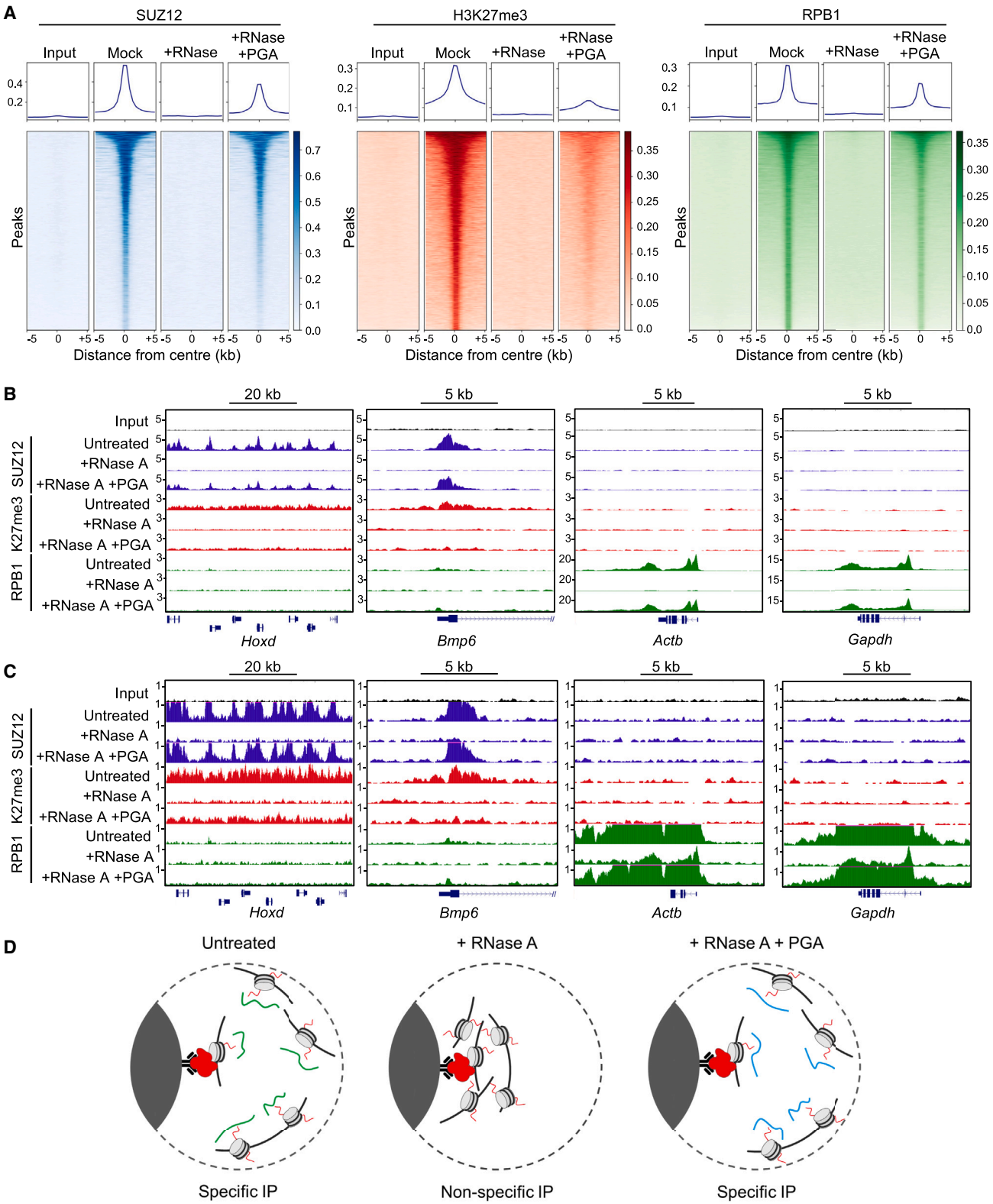

Figure 4. Apparent RNA-dependent PRC2 occupancy in rChIP experiments is due to non-specific chromatin IP

(A) Metagene plots (above) and heatmaps (below) of normalized reads (per million total reads) for input and SUZ12, H3K27me3, and RPB1 rChIP samples from mock-, RNase A-, or RNase A and PGA-treated sonicated crosslinked mESC extracts. For each epitope, normalized reads are shown centered on peaks called in

(legend continued on next page)

effect on H3K27me3, almost completely abrogating detection of H3K27me3-occupied sites (Figures 4A, 4B, and S1). Strikingly, the addition of PGA restored the detection of SUZ12 and H3K27me3 chromatin occupancy that was lost by RNase A treatment (Figures 4A, 4B, and S1).

In our hands, RNase A also strongly reduced the ChIP-seq signal for RPB1, and this too was substantially restored upon addition of PGA (Figures 4A and 4B). However, although much reduced, RPB1 occupancy was still evident at active genes in RNase A-treated samples (Figure 4C), especially in samples sonicated with the extended number of cycles used by Long et al. (Figure S1A).

Taking these sequencing results together with our other data, we conclude that the apparent loss of PRC2 chromatin occupancy caused by RNase A in rChIP experiments is due to the non-specific precipitation of chromatin that masks the enrichment of occupied genomic regions (Figure 4D). In the presence of RNA, sonicated chromatin fragments are held in solution allowing for specific IP of fragments bound by PRC2 or by other proteins of interest. In samples treated with RNase A, chromatin precipitates out of solution, and thus non-specific fragments co-precipitate with the fragments bound by the protein of interest, reducing their relative enrichment. The anionic polymer PGA maintains chromatin solubility in RNase A-treated samples, thus restoring IP specificity and the detection of bound genomic regions.

DISCUSSION

We report that experiments performed using rChIP methodology do not support a model in which RNA bridges PRC2 and chromatin. Rather than reducing the PRC2 ChIP-seq signal by severing an RNA bridge connecting PRC2 to chromatin, RNase A treatment of sonicated cell extracts causes non-specific chromatin precipitation, thereby diminishing the signal by increasing the background. This simple explanation also accounts for the loss of the H3K27me3 ChIP-seq signal upon RNase A treatment and for the restoration of both the PRC2 and H3K27me3 ChIP-seq signals by the addition of the anionic polymer PGA, neither of which can be explained by an RNA bridging model. Our results agree with those of a parallel independent study by Healy and colleagues,[30] who also demonstrate loss of ChIP specificity upon RNase A treatment when following the protocol of Long et al.

Our results are consistent with previous observations that RNase A treatment precipitates chromatin from sonicated cell extracts and that this could be rescued by the addition of PGA or other negatively charged polymers or by deleting positively charged histone tails.[28,29] Taken together with these previous studies, our results suggest that RNA prevents electrostatic aggregation of chromatin fragments in sonicated cell extracts. This interpretation is also consistent with the suggestion of Healy et al. that the absence of salt in the lysis buffer used in the rChIP protocol contributes to the apparent sensitivity of chromatin occupancy to RNA degradation.[30]

Our interpretation also accords with recent results presented by Long and colleagues.[31] The authors report that they observe increased chromatin precipitation when performing ChIP for PRC2 in the presence of RNase A but hypothesize that this is due to interaction of RNase A with chromatin rather than being caused by depletion of RNA. The authors also report that reducing the concentration of RNase A, or using an alternative enzyme, RNase T1, decreases this excess chromatin precipitation but still reduces PRC2 chromatin occupancy, albeit to less of an extent. However, these less-stringent RNase treatments are also shown to be less effective in depleting RNA, which explains the reduction in non-specific chromatin precipitation and, consequently, the more modest effect on enrichment of PRC2-bound chromatin versus the genomic background. Long and colleagues also report that RNA degradation has no effect on input DNA, but this would not be expected because input DNA is harvested without separation of soluble versus insoluble material.

Neither we nor Healy et al. have been able to reproduce the finding of Long et al. that RNase A has no effect on the ChIP-seq signal for RPB1, although our immunoblotting, ChIP-qPCR, and ChIP-seq data indicate that the detrimental effect of RNase A treatment on IP specificity is less severe for RPB1 than for PRC2 or H3K27me3. We speculate that differences in the degree of chromatin fragmentation, RNA degradation, or library fragment size could be responsible for the difference in results between our study and that of Long et al. We postulate that the milder effect on RPB1 is because active gene promoters contain nucleosome-depleted regions[32–34] and thus have a lower density of charged histones. CTCF occupancy at nucleosome-depleted regions[35,36] could also explain why the association of this factor with chromatin is also unaffected by RNA depletion.[31]

Limitations of the study

We performed three independent rChIP-qPCR and two independent rChIP-seq experiments. The two rChIP-seq experiments were performed under different conditions (20 sonication cycles and KAPA library preparation [Figure 4] versus 40 sonication cycles and NEB library preparation [Figure S1]) and thus cannot be considered direct replicates. However, we believe that observing

any one of the three conditions. In each heatmap, normalized reads are indicated by color, according to the scales on the right. Peaks are ordered by the average number of normalized reads.

(B) Genome browser snapshots of the *Hoxd* cluster, *Bmp6*, *Actb*, and *Gapdh* for the samples shown in (A). The y axis shows normalized reads (per million total reads).

(C) As (B) but with lower maximum y axis values to visualize RPB1 occupancy more clearly at *Gapdh* and *Actb* in RNase A-treated samples.

(D) Model. Left: in the presence of RNA (green), sonicated chromatin fragments are held in solution allowing for specific IP of PRC2-bound fragments. Middle: in samples treated with RNase A, non-specific fragments co-precipitate, reducing the relative enrichment of PRC2-bound genomic regions. This effect resembles the theoretical depletion of RNA-dependent PRC2 chromatin binding events. Right: the anionic polymer PGA (blue) maintains chromatin solubility in RNase A-treated samples, thereby restoring IP specificity and the detection of PRC2-bound genomic regions.

the same results (apparent loss of PRC2 and H3K27me3 occupancy upon RNA degradation and rescue of these effects with PGA) under different conditions provides greater confidence than direct replication of a single condition.

Although the apparent loss of PRC2 chromatin occupancy in rChIP experiments does not provide evidence for RNA bridges between PRC2 and its target sites on chromatin, we cannot rule out that RNA species protected from RNase A-mediated degradation perform this function. However, it is not necessary to invoke an RNA bridge model to explain PRC2 chromatin occupancy, which is dependent on recognition of H2AK119ub by JARID2 and of GC-rich DNA by PCL1-3.[10,11]

We also cannot rule out other mechanisms through which RNA may promote PRC2 chromatin association or activity. Long et al. reported that treatment of cells with the RNA polymerase II inhibitor triptolide depletes PRC2 from its target genes, but this effect was not observed in similar experiments by others,[37] and experiments performed by Long et al. may have been impacted by the chromatin precipitation that occurs in RNA-depleted lysates prepared in hypotonic buffer.[28,30]

We conclude that the apparent loss of PRC2 chromatin occupancy observed upon RNase A treatment of cell extracts in rChIP experiments does not reflect the severing of an RNA bridge but is instead a symptom of non-specific chromatin precipitation. Given the common utilization of RNase in studies probing the role of RNA in chromatin regulation,[38] our findings highlight the importance of ensuring that such experiments take electrostatic effects into account and are not affected by similar artifacts. We note that although the rChIP methodology produces experimental artifacts in its current form, it could still provide a means to identify RNA-dependent chromatin occupancy if performed in conditions that prevent chromatin precipitation upon RNA degradation.

STAR★METHODS

Detailed methods are provided in the online version of this paper and include the following:

- KEY RESOURCES TABLE
- RESOURCE AVAILABILITY
  - Lead contact
  - Materials availability
  - Data and code availability
- EXPERIMENTAL MODEL AND STUDY PARTICIPANT DETAILS
  - Cell lines
- METHOD DETAILS
  - rChIP
  - Separation of extracts into soluble and insoluble fractions
  - Co-immunoprecipitation
  - SDS-PAGE
  - Immunoblotting
  - DNA and RNA purification and agarose gel electrophoresis
  - qPCR
- QUANTIFICATION AND STATISTICAL ANALYSIS
  - RNA quantification
  - ChIP-qPCR
  - ChIP-seq

SUPPLEMENTAL INFORMATION

Supplemental information can be found online at https://doi.org/10.1016/j.celrep.2024.113856.

ACKNOWLEDGMENTS

We thank Chen Davidovich, Tom Cech, and John Rinn for discussions and for sharing unpublished data. Thanks to Yicheng Long and John Rinn for sharing the full rChIP protocol. This work was funded by a Cancer Research UK (CRUK) UCL Center (C416/A18088) PhD studentship and a grant from the Biotechnology and Biological Sciences Research Council (BB/W008750/1).

AUTHOR CONTRIBUTIONS

Investigation, A.H.H.; formal analysis, A.H.H.; data curation, A.H.H.; writing – original draft, A.H.H. and R.G.J.; writing – review & editing, A.H.H. and R.G.J.; conceptualization, R.G.J.; methodology, R.G.J.; supervision, R.G.J.

DECLARATION OF INTERESTS

The authors declare no competing interests.

Received: October 27, 2023
Revised: January 26, 2024
Accepted: February 8, 2024

REFERENCES

1. Janssen, S.M., and Lorincz, M.C. (2022). Interplay between chromatin marks in development and disease. Nat. Rev. Genet. *23*, 137–153. https://doi.org/10.1038/s41576-021-00416-x.
2. Helin, K., and Minucci, S. (2017). The Role of Chromatin-Associated Proteins in Cancer. Annu. Rev. Cancer Biol. *1*, 355–377. https://doi.org/10.1146/ANNUREV-CANCERBIO-050216-034422.
3. Nozawa, R.S., and Gilbert, N. (2019). RNA: Nuclear Glue for Folding the Genome. Trends Cell Biol. *29*, 201–211. https://doi.org/10.1016/J.TCB.2018.12.003.
4. Li, X., and Fu, X.D. (2019). Chromatin-associated RNAs as facilitators of functional genomic interactions. Nat. Rev. Genet. *20*, 503–519. https://doi.org/10.1038/s41576-019-0135-1.
5. Quinodoz, S.A., and Guttman, M. (2022). Essential Roles for RNA in Shaping Nuclear Organization. Cold Spring Harb. Perspect. Biol. *14*, a039719. https://doi.org/10.1101/CSHPERSPECT.A039719.
6. Long, Y., Wang, X., Youmans, D.T., and Cech, T.R. (2017). How do lncRNAs regulate transcription? Sci. Adv. *3*, eaao2110. https://doi.org/10.1126/SCIADV.AAO2110.
7. Skalska, L., Beltran-Nebot, M., Ule, J., and Jenner, R.G. (2017). Regulatory feedback from nascent RNA to chromatin and transcription. Nat. Rev. Mol. Cell Biol. *18*, 331–337. https://doi.org/10.1038/NRM.2017.12.
8. Almeida, M., Bowness, J.S., and Brockdorff, N. (2020). The many faces of Polycomb regulation by RNA. Curr. Opin. Genet. Dev. *61*, 53–61. https://doi.org/10.1016/J.GDE.2020.02.023.
9. Statello, L., Guo, C.J., Chen, L.L., and Huarte, M. (2021). Gene regulation by long non-coding RNAs and its biological functions. Nat. Rev. Mol. Cell Biol. *22*, 96–118. https://doi.org/10.1038/s41580-020-00315-9.
10. Blackledge, N.P., and Klose, R.J. (2021). The molecular principles of gene regulation by Polycomb repressive complexes. Nat. Rev. Mol. Cell Biol. *22*, 815–833. https://doi.org/10.1038/S41580-021-00398-Y.

11. Kim, J.J., and Kingston, R.E. (2022). Context-specific Polycomb mechanisms in development. Nat. Rev. Genet. *23*, 680–695. https://doi.org/10.1038/S41576-022-00499-0.

12. Rinn, J.L., Kertesz, M., Wang, J.K., Squazzo, S.L., Xu, X., Brugmann, S.A., Goodnough, L.H., Helms, J.A., Farnham, P.J., Segal, E., and Chang, H.Y. (2007). Functional Demarcation of Active and Silent Chromatin Domains in Human HOX Loci by Non-Coding RNAs. Cell *129*, 1311–1323. https://doi.org/10.1016/J.CELL.2007.05.022.

13. Zhao, J., Sun, B.K., Erwin, J.A., Song, J.J., and Lee, J.T. (2008). Polycomb proteins targeted by a short repeat RNA to the mouse X chromosome. Science *322*, 750–756. https://doi.org/10.1126/SCIENCE.1163045.

14. Pandey, R.R., Mondal, T., Mohammad, F., Enroth, S., Redrup, L., Komorowski, J., Nagano, T., Mancini-DiNardo, D., and Kanduri, C. (2008). Kcnq1ot1 antisense noncoding RNA mediates lineage-specific transcriptional silencing through chromatin-level regulation. Mol. Cell *32*, 232–246. https://doi.org/10.1016/J.MOLCEL.2008.08.022.

15. Khalil, A.M., Guttman, M., Huarte, M., Garber, M., Raj, A., Rivea Morales, D., Thomas, K., Presser, A., Bernstein, B.E., Van Oudenaarden, A., et al. (2009). Many human large intergenic noncoding RNAs associate with chromatin-modifying complexes and affect gene expression. Proc. Natl. Acad. Sci. USA *106*, 11667–11672. https://doi.org/10.1073/PNAS.0904715106.

16. Davidovich, C., Zheng, L., Goodrich, K.J., and Cech, T.R. (2013). Promiscuous RNA binding by Polycomb repressive complex 2. Nat. Struct. Mol. Biol. *20*, 1250–1257. https://doi.org/10.1038/NSMB.2679.

17. Beltran, M., Yates, C.M., Skalska, L., Dawson, M., Reis, F.P., Viiri, K., Fisher, C.L., Sibley, C.R., Foster, B.M., Bartke, T., et al. (2016). The interaction of PRC2 with RNA or chromatin is mutually antagonistic. Genome Res. *26*, 896–907. https://doi.org/10.1101/gr.197632.115.

18. Wang, X., Goodrich, K.J., Gooding, A.R., Naeem, H., Archer, S., Paucek, R.D., Youmans, D.T., Cech, T.R., and Davidovich, C. (2017). Targeting of Polycomb Repressive Complex 2 to RNA by Short Repeats of Consecutive Guanines. Mol. Cell *65*, 1056–1067.e5. https://doi.org/10.1016/j.molcel.2017.02.003.

19. Beltran, M., Tavares, M., Justin, N., Khandelwal, G., Ambrose, J., Foster, B.M., Worlock, K.B., Tvardovskiy, A., Kunzelmann, S., Herrero, J., et al. (2019). G-tract RNA removes Polycomb repressive complex 2 from genes. Nat. Struct. Mol. Biol. *26*, 899–909. https://doi.org/10.1038/s41594-019-0293-z.

20. Rosenberg, M., Blum, R., Kesner, B., Aeby, E., Garant, J.M., Szanto, A., and Lee, J.T. (2021). Motif-driven interactions between RNA and PRC2 are rheostats that regulate transcription elongation. Nat. Struct. Mol. Biol. *28*, 103–117. https://doi.org/10.1038/S41594-020-00535-9.

21. Kaneko, S., Son, J., Shen, S.S., Reinberg, D., and Bonasio, R. (2013). PRC2 binds active promoters and contacts nascent RNAs in embryonic stem cells. Nat. Struct. Mol. Biol. *20*, 1258–1264. https://doi.org/10.1038/NSMB.2700.

22. Kaneko, S., Son, J., Bonasio, R., Shen, S.S., and Reinberg, D. (2014). Nascent RNA interaction keeps PRC2 activity poised and in check. Genes Dev. *28*, 1983–1988. https://doi.org/10.1101/GAD.247940.114.

23. Cifuentes-Rojas, C., Hernandez, A.J., Sarma, K., and Lee, J.T. (2014). Regulatory interactions between RNA and polycomb repressive complex 2. Mol. Cell *55*, 171–185. https://doi.org/10.1016/J.MOLCEL.2014.05.009.

24. Herzog, V.A., Lempradl, A., Trupke, J., Okulski, H., Altmutter, C., Ruge, F., Boidol, B., Kubicek, S., Schmauss, G., Aumayr, K., et al. (2014). A strand-specific switch in noncoding transcription switches the function of a Polycomb/Trithorax response element. Nat. Genet. *46*, 973–981. https://doi.org/10.1038/NG.3058.

25. Wang, X., Paucek, R.D., Gooding, A.R., Brown, Z.Z., Ge, E.J., Muir, T.W., and Cech, T.R. (2017). Molecular analysis of PRC2 recruitment to DNA in chromatin and its inhibition by RNA. Nat. Struct. Mol. Biol. *24*, 1028–1038. https://doi.org/10.1038/NSMB.3487.

26. Zhang, Q., McKenzie, N.J., Warneford-Thomson, R., Gail, E.H., Flanigan, S.F., Owen, B.M., Lauman, R., Levina, V., Garcia, B.A., Schittenhelm, R.B., et al. (2019). RNA exploits an exposed regulatory site to inhibit the enzymatic activity of PRC2. Nat. Struct. Mol. Biol. *26*, 237–247. https://doi.org/10.1038/s41594-019-0197-y.

27. Long, Y., Hwang, T., Gooding, A.R., Goodrich, K.J., Rinn, J.L., and Cech, T.R. (2020). RNA is essential for PRC2 chromatin occupancy and function in human pluripotent stem cells. Nat. Genet. *52*, 931–938. https://doi.org/10.1038/s41588-020-0662-x.

28. Dueva, R., Akopyan, K., Pederiva, C., Trevisan, D., Dhanjal, S., Lindqvist, A., and Farnebo, M. (2019). Neutralization of the Positive Charges on Histone Tails by RNA Promotes an Open Chromatin Structure. Cell Chem. Biol. *26*, 1436–1449.e5. https://doi.org/10.1016/J.CHEMBIOL.2019.08.002.

29. Davie, J.R., and Candido, E.P. (1978). Acetylated histone H4 is preferentially associated with template active chromatin. Proc. Natl. Acad. Sci. USA *75*, 3574–3577. https://doi.org/10.1073/PNAS.75.8.3574.

30. Healy, E., Zhang, Q., Gail, E.H., Agius, S.C., Sun, G., Bullen, M., Pandey, V., Das, P.P., Polo, J.M., and Davidovich, C. (2023). The apparent loss of PRC2 chromatin occupancy as an artefact of RNA depletion. Preprint at bioRxiv. https://doi.org/10.1101/2023.08.16.553488.

31. Long, Y., Hwang, T., Gooding, A.R., Goodrich, K.J., Vallery, T.K., Rinn, J.L., and Cech, T.R. (2023). Evaluation of the RNA-dependence of PRC2 binding to chromatin in human pluripotent stem cells. Preprint at bioRxiv, 2023.08.17.553776. https://doi.org/10.1101/2023.08.17.553776.

32. Boeger, H., Griesenbeck, J., Strattan, J.S., and Kornberg, R.D. (2003). Nucleosomes unfold completely at a transcriptionally active promoter. Mol. Cell *11*, 1587–1598. https://doi.org/10.1016/S1097-2765(03)00231-4.

33. Bernstein, B.E., Liu, C.L., Humphrey, E.L., Perlstein, E.O., and Schreiber, S.L. (2004). Global nucleosome occupancy in yeast. Genome Biol. *5*, R62–R11. https://doi.org/10.1186/GB-2004-5-9-R62.

34. Lee, C.K., Shibata, Y., Rao, B., Strahl, B.D., and Lieb, J.D. (2004). Evidence for nucleosome depletion at active regulatory regions genome-wide. Nat. Genet. *36*, 900–905. https://doi.org/10.1038/NG1400.

35. Fu, Y., Sinha, M., Peterson, C.L., and Weng, Z. (2008). The Insulator Binding Protein CTCF Positions 20 Nucleosomes around Its Binding Sites across the Human Genome. PLoS Genet. *4*, 1000138. https://doi.org/10.1371/JOURNAL.PGEN.1000138.

36. Teif, V.B., Beshnova, D.A., Vainshtein, Y., Marth, C., Mallm, J.P., Höfer, T., and Rippe, K. (2014). Nucleosome repositioning links DNA (de)methylation and differential CTCF binding during stem cell development. Genome Res. *24*, 1285–1295. https://doi.org/10.1101/GR.164418.113.

37. Riising, E.M., Comet, I., Leblanc, B., Wu, X., Johansen, J.V., and Helin, K. (2014). Gene silencing triggers polycomb repressive complex 2 recruitment to CpG Islands genome wide. Mol. Cell *55*, 347–360. https://doi.org/10.1016/j.molcel.2014.06.005.

38. Thakur, J., and Henikoff, S. (2020). Architectural RNA in chromatin organization. Biochem. Soc. Trans. *48*, 1967–1978. https://doi.org/10.1042/BST20191226.

39. Hooper, M., Hardy, K., Handyside, A., Hunter, S., and Monk, M. (1987). HPRT-deficient (Lesch–Nyhan) mouse embryos derived from germline colonization by cultured cells. Nature, 292–295, 1987 326:6110 326. https://doi.org/10.1038/326292a0.

40. Ewels, P.A., Peltzer, A., Fillinger, S., Patel, H., Alneberg, J., Wilm, A., Garcia, M.U., Di Tommaso, P., and Nahnsen, S. (2020). The nf-core framework for community-curated bioinformatics pipelines. Nat. Biotechnol. *38*, 276–278. https://doi.org/10.1038/S41587-020-0439-X.

41. Li, H., and Durbin, R. (2009). Fast and accurate short read alignment with Burrows-Wheeler transform. Bioinformatics *25*, 1754–1760. https://doi.org/10.1093/BIOINFORMATICS/BTP324.

42. Danecek, P., Bonfield, J.K., Liddle, J., Marshall, J., Ohan, V., Pollard, M.O., Whitwham, A., Keane, T., McCarthy, S.A., Davies, R.M., and Li, H. (2021).

Twelve years of SAMtools and BCFtools. GigaScience *10*, giab008-4. https://doi.org/10.1093/GIGASCIENCE/GIAB008.

43. Zhang, Y., Liu, T., Meyer, C.A., Eeckhoute, J., Johnson, D.S., Bernstein, B.E., Nusbaum, C., Myers, R.M., Brown, M., Li, W., and Liu, X.S. (2008). Model-based analysis of ChIP-Seq (MACS). Genome Biol. *9*, R137–R139. https://doi.org/10.1186/GB-2008-9-9-R137/.
44. Quinlan, A.R., and Hall, I.M. (2010). BEDTools: a flexible suite of utilities for comparing genomic features. Bioinformatics *26*, 841–842. https://doi.org/10.1093/BIOINFORMATICS/BTQ033.
45. Ramírez, F., Dündar, F., Diehl, S., Grüning, B.A., and Manke, T. (2014). deepTools: a flexible platform for exploring deep-sequencing data. Nucleic Acids Res. *42*, W187–W191. https://doi.org/10.1093/NAR/GKU365.

STAR★METHODS

KEY RESOURCES TABLE

REAGENT or RESOURCE	SOURCE	IDENTIFIER
Antibodies		
Anti-H3	Abcam	Cat# ab1791; RRID:AB_302613
Anti-SUZ12	Cell Signaling	Cat#3737; RRID: AB_2536539
Anti-RPB1	Cell Signaling	Cat#14958; RRID: AB_2687876
Anti-EZH2	Cell Signaling	Cat# 5246; RRID:AB_10694683
Anti-SUZ12	Santa-Cruz	Cat# sc-271325; RRID:AB_10611204
Anti-β-Tubulin	Abcam	Cat# ab6046; RRID: AB_2210370
Anti-β-Actin	Cell Signaling	Cat# 4967S; RRID: AB_330288
Anti-H3K27me3	Abcam	Cat# ab192985; RRID: AB_2650559
Anti-H3K9me3	Abcam	Cat# ab8898; RRID: AB_306848
Anti-H3K27ac	Abcam	Cat# ab4729; RRID: AB_2118291
Anti-Rabbit-HRP	Dako	Cat# PO448
Anti-Mouse-HRP	Dako	Cat# PO260
Chemicals, peptides, and recombinant proteins		
Leukemia inhibitory factor (LIF)	Stemgent	Cat# 03-0011-100
RNase A	Thermo Scientific	Cat# EN0531
Poly-L-glutamic acid (PGA)	Sigma-Aldrich	Cat# P4761
Pierce protein A/G beads	Thermo Scientific	Cat# 88802
Oriole fluorescent gel stain	BioRad	Cat# 161-0496
Trizol-LS	ThermoFisher	Cat# 10296028
cOmplete protease inhibitor	Roche	Cat# 04693132001
Low range ssRNA ladder	NEB	Cat# N0364S
Critical commercial assays		
Qubit dsDNA Broad Range assay kit	ThermoFisher	Cat# Q32850
2100 Bioanalyzer High Sensitivity DNA kit	Agilent	Cat# 5067–4626
KAPA HyperPlus Kit	KAPA Biosystems	Cat# KK8512
NEBNext Ultra II DNA Library Prep Kit for Illumina	NEB	Cat# E7645S
SYBR Green Master Mix	Bio-Rad	Cat# 1725272
ECL	Bio-Rad	Cat# 170-5061
Qubit RNA Broad Range assay kit	ThermoFisher	Cat# Q10210
Agencourt AMPure XP beads	Beckman Coulter	Cat# A63880
Deposited data		
ChIP-seq data	This manuscript	GEO: GSE240380
Experimental models: Cell lines		
E14 mESC	(Hooper et al.)[39]	RRID: CVCL_C320
Oligonucleotides		
Hoxd11 F – GGCCGAGGGTTCTCCCCCTT	(Beltran et al.)[17]	N/A
Hoxd11 R – CCTCCCTCCCCCACCACCAG	(Beltran et al.)[17]	N/A
Actb F – AGGAGCTGCAAAGAAGCTGT	(Beltran et al.)[17]	N/A
Actb R – CCGCTGTGGCGTCCTATAAA	(Beltran et al.)[17]	N/A
Bmp6 F – AGCCGCCTCTGAGGGTTC	(Beltran et al.)[17]	N/A
Bmp6 R - GCCAGGTGTGTCCTAGGCAG	(Beltran et al.)[17]	N/A
Gapdh F – CCCACTCCGCGATTTTCA	This manuscript	N/A
Gapdh R – CTCTGCTCCTCCCTGTTCCA	This manuscript	N/A

(*Continued on next page*)

Continued

REAGENT or RESOURCE	SOURCE	IDENTIFIER
Software and algorithms		
ImageQuant TL software	GE Life Sciences	RRID: SCR_014246
DeepTools version 3.0.2	(Ramirez et al.)[45]	RRID: SCR_016366
NF-core ChIP-seq pipeline	(Ewels et al.)[40]	N/A
Graphpad Prism version 9.0	GraphPad Software	RRID: SCR_002798
MACS2	(Zhang et al.)[43]	RRID: SCR_013291
BWA	(Li et al.)[41]	RRID: SCR_010910
SAMtools	(Danecek et al.)[42]	RRID: SCR_002105

RESOURCE AVAILABILITY

Lead contact

Further Information and requests for resources and reagents should be directed to and will be fulfilled by the lead contact, Richard Jenner (r.jenner@ucl.ac.uk).

Materials availability

This study did not generate new unique reagents.

Data and code availability

- ChIP-seq data have been deposited at Gene Expression Omnibus (GEO) and are publicly available as of the date of publication. The accession number is listed in the key resources table.
- This paper does not report original code.
- Any additional information required to reanalyze the data reported in this paper is available from the lead contact upon request.

EXPERIMENTAL MODEL AND STUDY PARTICIPANT DETAILS

Cell lines

E14 mouse embryonic stem cells (mESC)[39] (male; gift from Helen Rowe) were used for all experiments. Cells were cultured on 0.1% gelatin coated dishes in KO-DMEM (ThermoFisher, 10829018), 10% FBS (ThermoFisher, A3160401), non-essential amino acids (ThermoFisher, 11140035), 2 mM L-glutamine (ThermoFisher, 25030–024), 50 μM 2-mercaptoethanol (ThermoFisher, 31350010), 100 U/mL penicillin-streptomycin (ThermoFisher, 15140–122), 1 mM sodium pyruvate (ThermoFisher, 11360039) and 1000 U/mL leukemia inhibitory factor (Stemgent, 03-0011-100). Media was changed every day and cells were split approximately every 48 h.

Cells were not authenticated. The cells tested negative for mycoplasma (Lonza, LT07-701).

METHOD DETAILS

Experiments were not performed blinded. Samples were not randomised.

rChIP

rChIP methodology was performed as described.[27] E14 cells were cultured on 15 cm plates until 80% confluency. Cells were harvested and washed in PBS before crosslinking in 1% formaldehyde in PBS for 10 min at room temperature (RT). Crosslinking was quenched by addition of 1/20th volume 2.5 M glycine followed by rotation for 10 min at RT. Cells were then washed twice in ice-cold PBS, flash frozen and stored at −80°C in 1x10^7 cell aliquots. Cells were resuspended in 500 μL lysis buffer (50 mM Tris-Cl pH 8.1, 10 mM EDTA, 0.5% SDS, plus protease inhibitor (cOmplete, EDTA-free Protease Inhibitor Cocktail (Roche, 04693132001) per 1.5 x10^7 cells. Cells were lysed on ice for 10 min prior to sonication for either 20 cycles (experiment 1) or 40 cycles (experiment 2; used by Long and colleagues[27]) of 30s on/30s off with a Bioruptor UCD-200 (Diagenode) at maximum power. Lysates were centrifuged at 17,000g for 10 min at 4°C, the supernatant collected and pre-cleared with 50 μL Pierce protein A/G magnetic beads (ThermoFisher 88802; pre-washed in IP buffer) per mL in IP buffer (16.7 mM Tris-HCl pH 8.1, 1.2 mM EDTA, 167 mM NaCl, 1% Triton X-100, cOmplete protease inhibitor) for 2 h at 4°C. Cell extract equivalent to 3 x10^6 cells per ChIP was diluted 1:5 in IP buffer and 2% taken and stored at −20°C as input. 2.5 μL anti-H3 (2.5 μg; Abcam, 1791), 2.5 μL anti-H3K27me3 (2.5 μg; Abcam, ab192985), 2.5 μL anti-SUZ12 (Cell Signaling, 3737) or 2.5 μL anti-RPB1 (Cell Signaling, 14958) antibody was added to the extracts, followed by incubation at 4°C overnight. For RNase A treated conditions, 5 μg/mL RNase A (Thermo Scientific, EN0531) was added together with the antibody, with or without the addition of 400 μg/mL PGA (Sigma-Aldrich, P4761). Following overnight incubation, 25 μL washed Pierce protein A/G beads were added and incubated for 1 h at RT. Beads were captured with a magnetic rack and washed twice

with 1 mL of each of the following buffers: low salt buffer (20 mM Tris-Cl pH 8.0, 2 mM EDTA, 150 mM NaCl, 0.1% SDS, 1% Triton X-100), high salt buffer (20 mM Tris-Cl pH 8.0, 2 mM EDTA, 500 mM NaCl, 0.1% SDS, 1% Triton X-100), LiCl buffer (10 mM Tris-Cl pH 8.0, 1 mM EDTA, 250 mM LiCl, 1% sodium deoxycholate, 1% IGEPAL CA-630 (Sigma-Aldrich, 6741), TE (10 mM Tris pH 8.0, 1 mM EDTA). Chromatin was eluted in 120 μL elution buffer (100 mM sodium bicarbonate, 1% SDS) for 20 min at RT. Input samples were thawed, topped up to 120 μL with elution buffer and incubated in parallel. Crosslinks were reversed through addition of NaCl (200 mM final) and incubation at 65°C overnight. RNA and protein were removed by incubation with 60 μg Proteinase K and 10 μg RNase A in 100 mM Tris-Cl (pH 8.0) and 10 mM EDTA at 37°C for 1 h. DNA was purified through phenol-chloroform-isoamyl extraction and ethanol precipitation with 200 mM NaCl and GlycoBlue (ThermoFisher, AM9516). DNA was resuspended in 30 μL 10 mM Tris-HCl, quantified using the Qubit dsDNA Broad Range assay kit (ThermoFisher, Q32850) and the size range determined on a Bioanalyser (Agilent). Specific DNA sequences were quantified by qPCR. Libraries were prepared from 2.5 ng of each sample using either the KAPA HyperPlus Kit (experiment 1: Roche/KAPA Biosystems, KK8512) or NEBNext Ultra II DNA Library Prep Kit for Illumina (experiment 2: NEB, E7645S), according to the manufacturers' protocols. DNA libraries were size selected for fragments between 150 and 800 bp using AMPure XP beads (Beckman Coulter, A63880). DNA libraries were pooled and sequenced with an Illumina NovaSeq (150 bp, paired end) by Novogene UK.

Separation of extracts into soluble and insoluble fractions

Extracts were prepared as above except lysates were sonicated for 12 cycles of 30s on/30s off, using a Bioruptor Pico (Diagenode). After incubation for 1 h at 4°C and then 1 h at RT with or without RNase A or PGA, extracts were centrifuged at 17,000g for 10 min at 4°C to separate soluble (supernatant) from insoluble (pellet) material.

Co-immunoprecipitation

Extracts were prepared as for rChIP except that lysates were sonicated for 12 cycles of 30s on/30s off, using a Bioruptor Pico (Diagenode). Sonicated extracts were diluted 1:5 in IP buffer (16.7 mM Tris-HCl pH 8.1, 1.2 mM EDTA, 167 mM NaCl, 1% Triton X-100, cOmplete protease inhibitor) with 2% extract (relative to the volume of an individual IP) removed as input. Extracts were split equally and incubated with 2.5 μL anti-H3 (2.5 μg; Abcam, 1791) 2.5 μL anti-SUZ12 (Cell Signaling, 3737) and 2.5 μL anti-RPB1 (Cell Signaling, 14958) antibody overnight at 4°C with or without RNase A before the addition of Pierce protein A/G beads and incubation for 1 h at RT. Beads were washed according to rChIP methodology and resuspended alongside inputs in NuPAGE LDS Sample Buffer (4X) (Invitrogen, NP0007) and incubated at 70°C for 10 min.

SDS-PAGE

Extracts were centrifuged at 16,000g for 10 min at 4°C to separate soluble (supernatant) from insoluble (pellet) material. The pellet was resuspended in an equal volume of 5:1 IP:lysis buffer. LDS sample buffer was added and proteins were resolved on 4–12% NuPAGE Bis-Tris precast gels (Life Technologies, NP0322) alongside PageRuler Plus Prestained Protein Ladder (Thermo Scientific, 26619). Proteins were visualised using Oriole fluorescent gel stain (Bio-Rad, 161–0496) and a BioRad ChemiDoc MP.

Immunoblotting

Proteins were transferred onto nitrocellulose membranes (Amersham, 10600002) in Tris-Glycine transfer buffer with 20% methanol. Membranes were blocked in TBS+0.1% Tween 20 (TBS-T) + 5% milk and then incubated overnight at 4°C with the following primary antibodies in TBS+5% milk: anti-RPB1 (1:1000; Cell Signaling, 14958), anti-EZH2 (1:1000; Cell Signaling, 5246), anti-SUZ12 (1:1000; Santa Cruz, sc-271325), anti-Beta-Tubulin (1:1000; Abcam, ab6046), anti-β-Actin (1:1000; Cell Signaling 4967S), anti-H3K9me3 (1:1000; Abcam, ab8898) anti-H3K27me3 (1:1000; Abcam, ab192985), anti-H3K27ac (1:1000; Abcam, ab4729) and anti-H3 (1:2000; Abcam, 1791). Membranes were washed 3x in TBS-T, incubated with HRP-conjugated goat anti-rabbit (Dako, P0448) or rabbit anti-mouse (Dako, PO260) secondary antibodies, washed again in TBS-T and proteins visualised with ECL (Biorad, 170–5061) and an Image Quant 800 (Amersham).

DNA and RNA purification and agarose gel electrophoresis

DNA was extracted from supernatants by addition of phenol:chloroform:isoamyl alcohol (25:24:1). The aqueous phase was isolated through centrifugation in MaXtract high density tubes (Qiagen, 50-727-738). DNA was precipitated at −20°C by the addition of 100% ethanol, NH_4OAc and GlycoBlue coprecipitant, washed in 80% ethanol and resuspended in TE. Equal volumes of DNA were loaded onto a 1.5% agarose gel and visualised using SYBR Safe nucleic acid gel stain (Invitrogen, S33102) and the UVP BioDoc-It Imaging System. After crosslink reversal and proteinase K treatment (3 h at 55°C), RNA was isolated using TRIzol LS Reagent (ThermoFisher, 10296028) in accordance with the manufacturer's instructions. Equal volumes of RNA were resolved on Novex TBE-urea gels (ThermoFisher, EC6865) alongside RNA size markers (NEB, N0364S) and visualised as for DNA. RNA concentration was measured using the Qubit RNA Broad Range assay kit (ThermoFisher, Q10210).

qPCR

qPCR was performed with SYBR Green Master Mix (Bio-Rad, 1725272) and the primers listed below in a QuantStudio 5 Real-Time PCR System (ThermoFisher) using the default program.

Primers (5′-3′):
Hoxd11 F – GGCCGAGGGTTCTCCCCCTT.
Hoxd11 R – CCTCCCTCCCCCACCACCAG.
Actb F – AGGAGCTGCAAAGAAGCTGT.
Actb R – CCGCTGTGGCGTCCTATAAA.
Bmp6 F – AGCCGCCTCTGAGGGTTC.
Bmp6 R - GCCAGGTGTGTCCTAGGCAG.
Gapdh F – CCCACTCCGCGATTTTCA.
Gapdh R – CTCTGCTCCTCCCTGTTCCA.

QUANTIFICATION AND STATISTICAL ANALYSIS

Statistical tests used and n are stated in the figure legends. No methods were used to determine whether the data met assumptions of the statistical approaches.

RNA quantification

Mean and standard error were calculated and plotted from triplicate experiments (3 independent mESC cultures) in Excel.

ChIP-qPCR

The amount of each DNA sequence in ChIP samples was calculated relative to input using the ΔCt method. Mean and standard error were calculated and plotted from triplicate experiments (3 independent mESC cultures) in Excel. The significance of differences in % input and ratio to *Gapdh* between each of the three conditions for each factor were estimated using one-sided unpaired t-tests with Excel (details in the Figure 3 legend).

ChIP-seq

Sequencing analysis was performed using the NF-core ChIP-seq pipeline.[40] Briefly, rChIP-seq reads were trimmed using trimgalore! and aligned to the reference genome GRCm38 using BWA (V 0.6.0).[41] Duplicates were removed using picard-tools, blacklisted regions were filtered and removed using SAMtools (v1.18)[42] and peaks called with MACS2 (3.0.0b2)[43] with the –broad option (default q-value of 0.05). Normalised bigwigs (reads per million mapped reads) were generated using BEDTools (v2)[44] and visualised using the UCSC genome browser. The sets of peaks called for each factor in each of the 3 conditions were combined and metaplots and heatmaps showing occupancy across these sets of combined peaks were generated with the computeMatrix and plotProfile/plotHeatmap functions from deepTools.[45] For experiment 2, H3K27me3 was plotted at SUZ12 peaks.